Spectrum of multispace Euclidean random matrices

Aldo Battista ⬤ and Rémi Monasson ⬤*

Laboratory of Physics of the Ecole Normale Supérieure, CNRS UMR 8023 & PSL Research,
Sorbonne Université, 24 rue Lhomond, 75005 Paris, France

We consider the additive superimposition of an extensive number of independent Euclidean Random Matrices in the high-density regime. The resolvent is computed with techniques from free probability theory, as well as with the replica method of statistical physics of disordered systems. Results for the spectrum and eigenmodes are shown for a few applications relevant to computational neuroscience, and are corroborated by numerical simulations.

I. INTRODUCTION

In the 20 years following their introduction, Euclidean random matrices (ERM) have been studied in a variety of contexts in physics [1,2] and mathematics [3–5]. Examples of applications of ERM include the theoretical description of vibrations in topologically disordered systems [6–8], wave propagation in random media [2,9], relaxation in glasses [10], Anderson localization [11], and many more [12].

While determining the spectral properties of ERM is generally quite involved due to the existence of correlations between the entries of these matrices, a well-understood limit is the so-called high-density regime [1,3]. Assume N points $\mathbf{r}_i$ are drawn uniformly at random in a bounded space, e.g., the unit D-dimensional hypercube $\mathcal{H}_D$, and define the N-dimensional ERM $\mathbf{M}^{(1)}$ with entries $M_{ij}^{(1)} = \Gamma(|\mathbf{r}_i - \mathbf{r}_j|)/N$. Here, $|\cdot|$ denotes the Euclidean distance (with periodic boundary conditions over $\mathcal{H}_D$), and Γ is a given function that depends only on the distance $|\cdot|$ and that has a finite range, independent of N. In the large-N limit (for fixed D), the points effectively form a dense, statistically uniform sampling of the hypercube; the eigenmodes of $\mathbf{M}^{(1)}$ are well approximated by Fourier plane waves [1,12], with eigenvalues

$$\hat{\Gamma}(\mathbf{k}) = \int_{\mathcal{H}_D} d\mathbf{r}\, e^{-i\,2\pi\,\mathbf{k}\cdot\mathbf{r}}\, \Gamma(|\mathbf{r}|), \qquad (1)$$

where the components of $\mathbf{k} = (k_1, k_2, \ldots, k_D)$ are integer valued.

Hereafter, we introduce a novel statistical ensemble of ERMs in the high-density regime obtained by mixing multiple spaces. Instead of having a single set of N random points $\mathbf{r}_i$, we consider L such sets, $\mathbf{r}_i^\ell$, with $\ell = 1, \ldots, L$ (and $i = 1, \ldots, N$ as usual). Each index ℓ points to a different "space" (hypercube), and for simplicity all points are drawn uniformly at random in the different spaces. We define the superimposition of all the ERM attached to the spaces, with entries

$$C_{ij} = \frac{1}{L} \sum_{\ell=1}^{L} \Gamma(|\mathbf{r}_i^\ell - \mathbf{r}_j^\ell|). \qquad (2)$$

We refer to such matrices as multispace ERM (MERM). To our knowledge, MERM have not been considered so far in statistical physics.

Our motivation to study MERM arises from computational neuroscience, more precisely, the need to understand how the hippocampal place-cell network can account for multiple cognitive maps, coding for various environmental and contextual situations. A review on place cells and the representation of space in the hippocampus can be found in Ref. [13]. From a model perspective the points $\mathbf{r}_i^\ell$ correspond to the positions of the centers of the place field of place cell i in map ℓ. The resulting statistical ensemble for MERM is sketched in Fig. 1. An important issue is the maximal number L of maps the hippocampal recurrent neural network (with N neurons) can sustain, more precisely, the maximal ratio

$$\alpha = \frac{L}{N}, \qquad (3)$$

called critical capacity. This capacity depends on the dimension of the maps, $D \ll N$, and of their spatial accuracy (the precision with which N-dimensional neural configurations encode D-dimensional positions along the map). In a recent work, we have shown how the critical capacity could be determined from the knowledge of the resolvent of $\mathbf{C}$ [14]. A nontrivial statistical setting is obtained when the number L of spaces is of the order of the matrix size, N. More precisely, we consider herefater the double infinite size limit $L, N \to \infty$ at fixed ratio α. This choice corresponds to the assumption that the hippocampal network activity can code for many different environments [15] or different contexts [16], and operates, as hypothesized for other cortical areas [17], in a regime close to maximal capacity.

Our paper is organized as follows. The spectrum of MERM is computed using arguments borrowed from free probability theory in Sec. II, and rederived using the replica method in Sec. III. We show the results for the spectrum and eigenmodes for the choice of Γ corresponding to Fig. 1 and compare with
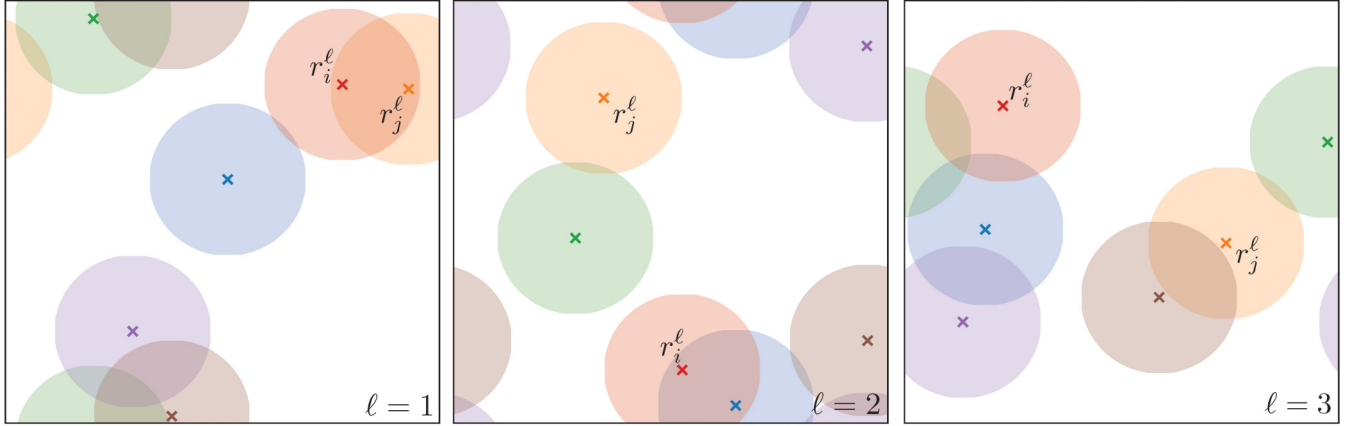
*monasson@lpt.ens.fr

FIG. 1. Basic statistical ensemble of MERM considered in this work. $L = 3$ sets of $N = 5$ points, $\mathbf{r}_i^\ell$, with $\ell = 1, \ldots, L$ and $i = 1, \ldots, N$ are drawn uniformly at random in unit squares $\mathcal{H}_2$ (dimension $D = 2$). Points are represented by crosses, whose colors identify their indices i. The MERM is defined through (2), where Γ is a generic function of the distance between points, see main text. A possible choice for Γ, inspired from the so-called place cells in neuroscience, is the overlap (common area) between pairs of disks of surface $\phi_0 < 1$ and having centers $\mathbf{r}_i^\ell$ in each space ℓ.

numerical simulations in Sec. IV. Variations on the choice of Γ are discussed in Sec. V. Last, Sec. VI presents some conclusions.

II. SPECTRUM OF MERM: FREE-PROBABILITY-INSPIRED DERIVATION

Let us consider an extensive number L of spaces, see (3), with

$$M_{ij}^{(L)} = \frac{1}{N} \sum_{\ell=1}^{L} \Gamma\big(|\mathbf{r}_i^\ell - \mathbf{r}_j^\ell|\big), \tag{4}$$

where the points are independently drawn from one space ℓ to another and where the single elements of the sum are ERM defined from N points $\mathbf{r}_i^\ell$ drawn uniformly at random in the D-dimensional unit hypercube $\mathcal{H}_D$:

$$M_{ij}^{(1)} = \frac{1}{N} \Gamma\big(|\mathbf{r}_i^\ell - \mathbf{r}_j^\ell|\big). \tag{5}$$

A. Case of the extensive eigenvalue: $\mathbf{k = 0}$

We compute the resolvent (Stieltjes transform) of $\mathbf{M}^{(L)}$ using free-probability arguments [18,19]. Heuristically, asymptotic freeness between the different ERMs relies on the fact that their eigenvectors basis are mutually incoherent. In the $N \to \infty$ limit, the eigenvalues of $\mathbf{M}^{(1)}$ in space ℓ are the Fourier coefficients (1) of Γ, where $\mathbf{k} \in \mathbb{Z}^D$ and the associated eigenvectors have components $v_i(\mathbf{k}) \simeq e^{i 2\pi \, \mathbf{k} \cdot \mathbf{r}_i^\ell}/\sqrt{N}$ [1,3,12]. All ERMs defined in the sum in (4) have mutually incoherent eigenbasis only if we restrict the analysis to the subspace orthogonal to the uniform mode attached to $\mathbf{k = 0}$, shared by all the spaces. Though this argument is not rigorous, we expect this restriction to allow us to find all the eigenvalues of $\mathbf{M}^{(L)}$, except the one corresponding to the asymptotically uniform eigenvector.

Furthermore it is easy to determine the leading behavior (when N is large) of the eigenvalue of $\mathbf{M}^{(L)}$ corresponding to $\mathbf{k = 0}$. As the corresponding eigenvector is expected to have all components equal to $N^{-1/2}$, we find that the corresponding eigenvalue is extensive in N and approximately equal to $\Lambda = N \alpha \, \hat{\Gamma}(\mathbf{0})$. For the matrix $\mathbf{C}$ the corresponding eigenvalue is $z_{\text{ext}} = \frac{\Lambda}{\alpha} = N \, \hat{\Gamma}(\mathbf{0})$.

From now on we concentrate on calculating the spectrum of $\mathbf{M}^{(L)}$ corresponding to $\mathbf{k \neq 0}$; the term "resolvent" will refer to the resolvent in the $\mathbf{k \neq 0}$ subspace.

B. Case of a single space ($L = 1$)

The resolvent of $\mathbf{M}^{(1)}$ is defined as

$$s_1(z) = \frac{1}{N} \langle \text{Trace} \, (\mathbf{M}^{(1)} - z \, \mathbf{Id})^{-1} \rangle_{(1)}, \tag{6}$$

where $\langle \cdot \rangle_{(1)}$ stands for the average over the distribution of the matrix (5). It is easy to rewrite the resolvent when $N \gg 1$,

$$s_1(z) = -\frac{1}{zN}\left[N + \sum_{\ell=1}^{\infty} \sum_{\substack{\mathbf{k} \neq \mathbf{0} \\ (|\mathbf{k}| \leqslant N)}} \hat{\Gamma}(\mathbf{k})^\ell \frac{1}{z^\ell} \right]$$

$$= -\frac{1}{z} - \frac{1}{N z} \gamma\left(\frac{1}{z}\right) \tag{7}$$

with

$$\gamma(u) = \sum_{\mathbf{k} \neq \mathbf{0}} \frac{u \, \hat{\Gamma}(\mathbf{k})}{1 - u \, \hat{\Gamma}(\mathbf{k})} \tag{8}$$

and where the sum runs over $\mathbb{Z}^D$ without the $\mathbf{k \neq 0}$ term.

C. Case of multiple spaces ($L = \alpha N$)

We now consider the case of $\mathbf{M}^{(L)}$. Its resolvent $s_L(z)$ is defined as

$$s_L(z) = \frac{1}{N} \langle \text{Trace} \, (\mathbf{M}^{(L)} - z \, \mathbf{Id})^{-1} \rangle_{(L)}, \tag{9}$$

where $\langle \cdot \rangle_{(L)}$ stands for the average over the distribution of the matrix (4), can be computed through the following steps:

(i) Invert (functionally) the resolvent $s_1(z)$ of $\mathbf{M}^{(1)}$: We first rewrite (7) into the following implicit equation for the inverse resolvent:

$$z_1(s) = -\frac{1}{s} - \frac{1}{N\,s}\,\gamma\left[\frac{1}{z_1(s)}\right]. \qquad (10)$$

We then send N to infinity in the above equation, and obtain that $z_1(s) = -1/s$ in this limit. Using this expression for the argument of the γ function in (10) we obtain the $\frac{1}{N}$ correction to the inverse resolvent:

$$z_1(s) = -\frac{1}{s} - \frac{\gamma(-s)}{N\,s}. \qquad (11)$$

(ii) Compute the R transform of $\mathbf{M}^{(1)}$, defined through

$$R_1(s) \equiv z_1(-s) - \frac{1}{s}. \qquad (12)$$

Note the unusual presence of a minus sign in the argument of z_1 in the above equation, due to the fact that our resolvent is defined as the opposite of the standard resolvent [18]. Using (11), we obtain

$$R_1(s) = \frac{\gamma(s)}{N\,s} + o\left(\frac{1}{N}\right). \qquad (13)$$

(iii) Compute the R transform of $\mathbf{M}^{(L)}$ through

$$R_L(s) = L\,R_1(s). \qquad (14)$$

Using (13), we obtain

$$R_L(s) = \alpha\,\frac{\gamma(s)}{s} + o(1), \qquad (15)$$

where the corrections $o(1)$ vanish when both $N, L \to \infty$ at fixed ratio α.

(iv) Write the functional inverse resolvent of $\mathbf{M}^{(L)}$ through

$$z_L(s) = R_L(-s) - \frac{1}{s} = -\frac{1 + \alpha\,\gamma(-s)}{s}. \qquad (16)$$

(vi) Compute the resolvent $s_L(z)$ of $\mathbf{M}^{(L)}$. From (16) and (8) we find the implicit equation satisfied by s_L:

$$z = \alpha \sum_{\mathbf{k} \neq \mathbf{0}} \frac{\hat{\Gamma}(\mathbf{k})}{1 + s_L\,\hat{\Gamma}(\mathbf{k})} - \frac{1}{s_L}. \qquad (17)$$

Note that we are eventually interested in the spectral properties of the matrix $\mathbf{C}$ with entries

$$C_{ij} = \frac{1}{L} \sum_{\ell=1}^{L} \Gamma\left(|\mathbf{r}_i^\ell - \mathbf{r}_j^\ell|\right) = \frac{1}{\alpha} M_{ij}^{(L)}. \qquad (18)$$

Obviously, the resolvent s of $\mathbf{C}$ is related to the resolvent s_L of $\mathbf{M}^{(L)}$ through the equation $s(z) = \alpha\,s_L(\alpha z)$. Hence we obtain our fundamental implicit equation for the resolvent of $\mathbf{C}$:

$$z = \sum_{\mathbf{k} \neq \mathbf{0}} \frac{\alpha\,\hat{\Gamma}(\mathbf{k})}{\alpha + s\,\hat{\Gamma}(\mathbf{k})} - \frac{1}{s}. \qquad (19)$$

III. SPECTRUM OF MERM: REPLICA-BASED DERIVATION

Here we rederive the implicit equation (17) for the resolvent of $\mathbf{M}^{(L)}$ defined in (9) using the replica method coming

from statistical physics of disordered systems. We start by rewriting the definition of the resolvent as

$$s_L(z) = \frac{2}{N} \partial_z \langle \log \det[\mathbf{M}^{(L)} - z\,\mathbf{Id}]^{-\frac{1}{2}} \rangle_{(L)}, \qquad (20)$$

where $\langle \cdot \rangle_{(L)}$ it is still the average over the distribution of the matrix (4). With this representation the determinant $\det\left[\mathbf{M}^{(L)} - z\,\mathbf{Id}\right]^{-\frac{1}{2}}$ can be expressed as a canonical partition function:

$$\begin{aligned}
\mathcal{Z}_L(s) &= \det[\mathbf{M}^{(L)} - z\,\mathbf{Id}]^{-\frac{1}{2}} \\
&= \int \prod_i \frac{d\phi_i}{\sqrt{2\pi}} \exp\left[\frac{z}{2} \sum_i \phi_i^2 - \frac{1}{2} \sum_{ij} \phi_i M_{ij}^{(L)} \phi_j\right],
\end{aligned}$$
$$(21)$$

where i, j go from 1 to N. Notice that it is legit to adopt a real-valued Gaussian representation for the inverse square root of the determinant. Each ERM $\mathbf{M}^{(1)}$ is a correlation matrix, and have real, non-negative eigenvalues; consequently, $\mathbf{M}^{(L)}$, which is the sum of correlation matrices, also has real and non-negative eigenvalues.

Resolvent (20) can be calculated using the replica trick [20]:

$$s_L(z) = \frac{2}{N} \partial_z \langle \log \mathcal{Z}_L(s) \rangle_{(L)} = \frac{2}{N} \partial_z \left[\lim_{n \to 0} \frac{1}{n} \log \langle \mathcal{Z}_L(s)^n \rangle_{(L)}\right]$$
$$(22)$$

with

$$\begin{aligned}
\langle \mathcal{Z}_L(s)^n \rangle_{(L)} &= \int \prod_{ia} \frac{d\phi_i^a}{\sqrt{2\pi}} \exp\left[\frac{z}{2} \sum_a \sum_i \left(\phi_i^a\right)^2\right] \\
&\times \left\langle \exp\left[-\frac{1}{2} \sum_a \sum_{ij} \phi_i^a M_{ij}^{(L)} \phi_j^a\right]\right\rangle_{(L)}, \quad (23)
\end{aligned}$$

where we have replicated the system n times, i.e., a goes from 1 to n.

In order to perform the average in (23) we rewrite (4) by considering the ℓth space ERM in its eigenbasis:

$$M_{ij}^{(L)} = \frac{1}{N} \sum_{\ell=1}^{L} \Gamma\left(|\mathbf{r}_i^\ell - \mathbf{r}_j^\ell|\right) = \sum_\ell \sum_{\mathbf{k} \neq \mathbf{0}} v_{\mathbf{k}i}^\ell\,\hat{\Gamma}(\mathbf{k})\,v_{\mathbf{k}j}^\ell, \quad (24)$$

where ℓ goes from 1 to L, and the sum over $\mathbf{k}$ discards the $\mathbf{k} = \mathbf{0}$ extensive mode because as discussed in the previous section. The eigenvector components, $v_{\mathbf{k}i}^\ell \simeq \frac{1}{\sqrt{N}} \sin\left(2\pi\,\mathbf{k} \cdot \mathbf{r}_i^\ell\right)$, $\frac{1}{\sqrt{N}} \cos\left(2\pi\,\mathbf{k} \cdot \mathbf{r}_i^\ell\right)$, are real due to the symmetry $\hat{\Gamma}(\mathbf{k}) = \hat{\Gamma}(-\mathbf{k})$. Hence we get

$$\begin{aligned}
&\left\langle \exp\left[-\frac{1}{2} \sum_a \sum_{ij} \phi_i^a M_{ij}^{(L)} \phi_j^a\right]\right\rangle_{(L)} \\
&= \left\langle \exp\left[-\frac{1}{2} \sum_{a,\ell,\mathbf{k} \neq \mathbf{0}} \hat{\Gamma}(\mathbf{k}) \left(\sum_i v_{\mathbf{k}i}^\ell \phi_i^a\right)^2\right]\right\rangle_{(L)}. \quad (25)
\end{aligned}$$

We now use the Stratonovich trick to linearize $(\sum_i v^\ell_{\mathbf{k}i} \phi^a_i)^2$:

$$
\left\langle \exp\left[-\frac{1}{2} \sum_{a,\ell,\mathbf{k}\neq\mathbf{0}} \hat{\Gamma}(\mathbf{k}) \left(\sum_i v^\ell_{\mathbf{k}i} \phi^a_i \right)^2 \right] \right\rangle_{(L)}
$$

$$
= \prod_\ell \int \prod_{a,\mathbf{k}\neq\mathbf{0}} \frac{du^a_{\ell,\mathbf{k}}}{\sqrt{2\pi}} \exp\left[-\frac{1}{2} \sum_{a,\mathbf{k}\neq\mathbf{0}} (u^a_{\ell,\mathbf{k}})^2 \right]
$$

$$
\times \left\langle \exp\left[-i \sum_{a,\mathbf{k}\neq\mathbf{0}} \sqrt{\hat{\Gamma}(\mathbf{k})}\, u^a_{\ell\mathbf{k}} \sum_i \phi^a_i v^\ell_{\mathbf{k}i} \right] \right\rangle_{(L)}. \quad (26)
$$

Using the fact that $\langle v^\ell_{\mathbf{k}i} \rangle = 0$ and $\langle v^\ell_{\mathbf{k}i} v^\ell_{\mathbf{k}'j} \rangle = \frac{1}{N} \delta_{ij}\delta_{\mathbf{k}\mathbf{k}'}$ it is easy to perform the average in the above equation, with the result

$$
\left\langle \exp\left[-i \sum_{a,\mathbf{k}\neq\mathbf{0}} \sqrt{\hat{\Gamma}(\mathbf{k})}\, u^a_{\ell\mathbf{k}} \sum_i \phi^a_i v^\ell_{\mathbf{k}i} \right] \right\rangle_{(L)}
$$

$$
= \exp\left[-\frac{1}{2} \sum_{a,b} \sum_{\mathbf{k}\neq\mathbf{0}} \hat{\Gamma}(\mathbf{k}) q^{ab} u^a_{\ell\mathbf{k}} u^b_{\ell\mathbf{k}} \right], \quad (27)
$$

where we have defined the overlap q^{ab} as

$$
q^{ab} = \frac{1}{N} \sum_i \phi^a_i \phi^b_i \quad (28)
$$

to be fixed through

$$
1 = \int \prod_{a\leqslant b} \frac{d\hat{q}^{ab} dq^{ab}}{\frac{2\pi i}{N}} \exp\left(N \sum_{a\leqslant b} \hat{q}^{ab} q^{ab} - \sum_{a\leqslant b} \hat{q}^{ab} \sum_i \phi^a_i \phi^b_i \right). \quad (29)
$$

We can finally write $\langle \mathcal{Z}_L(s)^n \rangle_{(L)}$ as

$$
\langle \mathcal{Z}_L(s)^n \rangle_{(L)} = \int \prod_{a\leqslant b} \frac{d\hat{q}^{ab} dq^{ab}}{\frac{2\pi i}{N}} \exp\left(N \left\{ \log \int \prod_a \frac{d\phi^a}{\sqrt{2\pi}} \right. \right.
$$

$$
\times \exp\left[\frac{z}{2} \sum_a (\phi^a)^2 - \sum_{a\leqslant b} \hat{q}^{ab} \phi^a \phi^b \right]
$$

$$
+ \sum_{a\leqslant b} \hat{q}^{ab} q^{ab} + \alpha \log \int \prod_{\mathbf{k}\neq\mathbf{0},a} \frac{du^a_{\mathbf{k}}}{\sqrt{2\pi}}
$$

$$
\times \exp\left[-\frac{1}{2} \sum_{\mathbf{k}\neq\mathbf{0},a} (u^a_{\mathbf{k}})^2 \right.
$$

$$
\left. \left. \left. -\frac{1}{2} \sum_{\mathbf{k}\neq\mathbf{0}} \sum_{a\leqslant b} \hat{\Gamma}(\mathbf{k}) q^{ab} u^a_{\mathbf{k}} u^b_{\mathbf{k}} \right] \right\} \right). \quad (30)
$$

The Gaussian integrals over ϕ^a and $u^a_{\mathbf{k}}$ can be easily computed. We then make the replica symmetric (RS) ansatz on the structure of the order parameters q^{ab} and their conjugate variables $\hat{q}^{ab}$, so that

$$
q^{ab} = r + (q-r)\delta_{ab} \quad (31)
$$

and

$$
\hat{q}^{ab} = \hat{r} + (\hat{q}-\hat{r})\delta_{ab}. \quad (32)
$$

The integrals over q, r, $\hat{q}$, and $\hat{r}$ are then estimated using the saddle-point method valid for large N, and then taking the small-n limit. The resulting expression for the resolvent of (4) is

$$
s_L(z) = 2\partial_z \left[\text{opt}_{q,r,\hat{q},\hat{r}} \lim_{n\to 0} \lim_{N\to\infty} \frac{1}{nN} \log\langle \mathcal{Z}_L(s)^n \rangle_{(L)} \right]
$$

$$
= 2\partial_z[\text{opt}_{q,r,\hat{q},\hat{r}} f(q,r,\hat{q},\hat{r})], \quad (33)
$$

where f is the free energy density equal to

$$
f(q,r,\hat{q},\hat{r}) = \hat{q}q - \frac{1}{2}\hat{r}r - \frac{\alpha}{2} \sum_{\mathbf{k}\neq\mathbf{0}} \left\{ \log[1 + \hat{\Gamma}(\mathbf{k})(q-r)] \right.
$$

$$
\left. + \frac{\hat{\Gamma}(\mathbf{k})r}{1 + \hat{\Gamma}(\mathbf{k})(q-r)} \right\} - \frac{1}{2}\log(2\hat{q} - \hat{r} - z)
$$

$$
- \frac{\hat{r}}{2(2\hat{q} - \hat{r} - z)}. \quad (34)
$$

The saddle-point equations obtained by optimizing $f(q,r,\hat{q},\hat{r})$ with respect to $\hat{q}$, $\hat{r}$, q, and r read

$$
q = -\frac{\hat{r}}{(2\hat{q} - \hat{r} - z)^2} + \frac{1}{2\hat{q} - \hat{r} - z}, \quad r = -\frac{\hat{r}}{(2\hat{q} - \hat{r} - z)^2},
$$

$$
\hat{q} = \frac{\alpha}{2} \sum_{\mathbf{k}\neq\mathbf{0}} \left\{ \frac{\hat{\Gamma}(\mathbf{k})}{1 + \hat{\Gamma}(\mathbf{k})(q-r)} - \frac{r\,\hat{\Gamma}(\mathbf{k})^2}{[1 + \hat{\Gamma}(\mathbf{k})(q-r)]^2} \right\},
$$

$$
\hat{r} = -\alpha \sum_{\mathbf{k}\neq\mathbf{0}} \frac{r\,\hat{\Gamma}(\mathbf{k})^2}{[1 + \hat{\Gamma}(\mathbf{k})(q-r)]^2}. \quad (35)
$$

This system of equations admits $r = \hat{r} = 0$ as a solution, which gives, according to (33), the following implicit equation satisfied by $s_L(z)$:

$$
z = \alpha \sum_{\mathbf{k}\neq\mathbf{0}} \frac{\hat{\Gamma}(\mathbf{k})}{1 + s_L \hat{\Gamma}(\mathbf{k})} - \frac{1}{s_L}. \quad (36)
$$

This equation is identical to (17) obtained using free probability theory.

IV. APPLICATION AND COMPARISON WITH NUMERICS

A. Numerical computation of the spectrum

We now aim at solving the implicit equation (19) satisfied by the resolvent of **C**. We show in Fig. 2(a) the representative curve of z as a function of s around the pole at the origin ($s = 0$). A set of forbidden disjoint intervals, $z \in [z^{(m)}_-, z^{(m)}_+]$, with $m = 1, \ldots, M$ is found, which cannot be reached for real-valued s; the number M of these intervals is a decreasing function of the ratio α. When z lies in one of these intervals, we look for a solution to Eq. (19) with

$$
s = s_r + i\,s_i, \quad (37)
$$

where the imaginary part s_i is strictly positive. For $z = x + i\epsilon$, the density of eigenvalues at x is given by $\rho(x) = \lim_{\epsilon\to 0} s_i(z)/\pi$ by virtue of well-known properties of the Stieljes transform. From now on we will indicate with z the
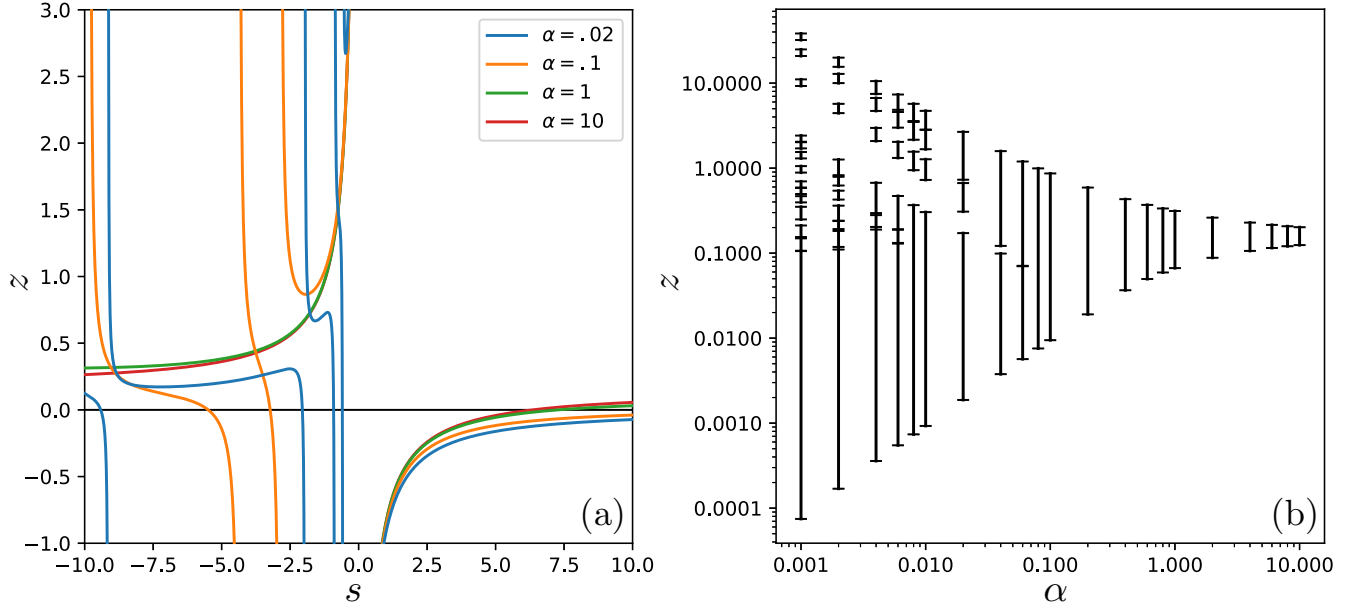
FIG. 2. (a) z vs. s, see (19), close to the origin ($s = 0$), for different values of α. (b) Support of the spectrum for different values of α: black segments show the interval of eigenvalues z with nonzero density $\rho(z)$. Results obtained by taking for Γ the overlap (common length) between segments of length $\phi_0 = .2$, centered in points $\mathbf{r}_i^\ell$ randomly drawn in the unit interval $\mathcal{H}_1$ ($D = 1$), more precisely $\Gamma(|\mathbf{r}_i^\ell - \mathbf{r}_j^\ell|) = \phi_0 - |\mathbf{r}_i^\ell - \mathbf{r}_j^\ell|$.

eigenvalue and with $\rho(z)$ the correspondent density, bearing in mind the $\epsilon \to 0$ limit.

The implicit equations fulfilled by s_r and s_i for $z \in [z_-^{(m)}, z_+^{(m)}]$, with $m = 1, \ldots, M$ read

$$z = \sum_{\mathbf{k} \neq \mathbf{0}} \frac{\alpha^2 \, \hat{\Gamma}(\mathbf{k})}{[\alpha + s_r \, \hat{\Gamma}(\mathbf{k})]^2 + [s_i \, \hat{\Gamma}(\mathbf{k})]^2}, \tag{38}$$

$$\frac{1}{s_r^2 + s_i^2} = \sum_{\mathbf{k} \neq \mathbf{0}} \frac{\alpha \, \hat{\Gamma}(\mathbf{k})^2}{[\alpha + s_r \, \hat{\Gamma}(\mathbf{k})]^2 + [s_i \, \hat{\Gamma}(\mathbf{k})]^2}, \tag{39}$$

and can be solved numerically. Figure 3 shows the density of eigenvalues for various values of α. We observe the presence of the disconnected intervals $[z_-^{(m)}; z_+^{(m)}]$ corresponding to nonzero density $\rho(z)$, referred to as "connected components" below. These connected components originate from the discrete spectrum of ERM (with eigenvalues labeled by $\mathbf{k}$) and progressively merge as α increases [Fig. 2(b)]. We now discuss the mechanism leading to merging in the large $|\mathbf{k}|$, small-α regime.

B. Merging of density "connected components": Behavior of the density at small α

For small α, we look for a solution of Eq. (19) near the poles, so that to consider only a value $\mathbf{k} \neq \mathbf{0}$ in the sum over the modes:

$$z(\mathbf{k}) = \frac{\alpha \, \hat{\Gamma}(\mathbf{k})}{\alpha + s(\mathbf{k}) \, \hat{\Gamma}(\mathbf{k})} - \frac{1}{s(\mathbf{k})}. \tag{40}$$

We find then $s(\mathbf{k})$ such that $\frac{dz(\mathbf{k})}{ds(\mathbf{k})} = 0$, i.e., where the resolvent has singularities (eigenvalues), obtaining:

$$s_\pm(\mathbf{k}) = -\frac{\alpha}{\hat{\Gamma}(\mathbf{k})}(1 \pm \sqrt{\alpha}), \tag{41}$$

this implies that the spectrum has the edges located at:

$$z_\pm(\mathbf{k}) = \frac{\hat{\Gamma}(\mathbf{k})}{\alpha}(1 \pm 2\sqrt{\alpha}). \tag{42}$$

This means that when α become sufficiently small the spectrum develop a connected component in correspondence of every $\mathbf{k} \neq \mathbf{0}$ centered in $z_{\mathbf{k}} = \frac{1}{2}[z_-(\mathbf{k}) + z_+(\mathbf{k})] = \frac{\hat{\Gamma}(\mathbf{k})}{\alpha}$ and of half-width $\frac{1}{2}[z_+(\mathbf{k}) - z_-(\mathbf{k})] = \frac{2\hat{\Gamma}(\mathbf{k})}{\sqrt{\alpha}}$. In order now to understand how the density of eigenvalues behaves inside these connected components we look to a solution of equation (40) of the form

$$s(\mathbf{k}) = s_r(\mathbf{k}) + i \, s_i(\mathbf{k}), \tag{43}$$

so that to finally obtain the parametric equations for the density $\rho(z)$ of eigenvalues equal to z:

$$\rho(x; \mathbf{k}) = \frac{\alpha^{\frac{3}{2}}}{\pi \hat{\Gamma}(\mathbf{k})} \sqrt{1 - x^2}, \quad z(x; \mathbf{k}) = \frac{\hat{\Gamma}(\mathbf{k})}{\alpha}(1 + 2x\sqrt{\alpha}), \tag{44}$$

where $x \in [-1; 1]$. This solution makes sense only for the modes $\mathbf{k}$ and ratios α such that the local semicircle distributions attached to two contiguous eigenvalues do not overlap. More precisely, the ratio α should be smaller than

$$\alpha_{\mathrm{merging}}(\mathbf{k}) \simeq \frac{[\hat{\Gamma}(\mathbf{k}) - \hat{\Gamma}(\mathbf{k}^c)]^2}{4[\hat{\Gamma}(\mathbf{k}) + \hat{\Gamma}(\mathbf{k}^c)]^2}, \tag{45}$$

where $\mathbf{k}^c$ is the momentum vector corresponding to the closest eigenvalue to $\hat{\Gamma}(\mathbf{k})$. This formula gives the values of the ratios at which the small connected components of $\rho(z)$ [Figs. 2(b) and 3] successively merge and is asymptotically correct for large $|\mathbf{k}|$.
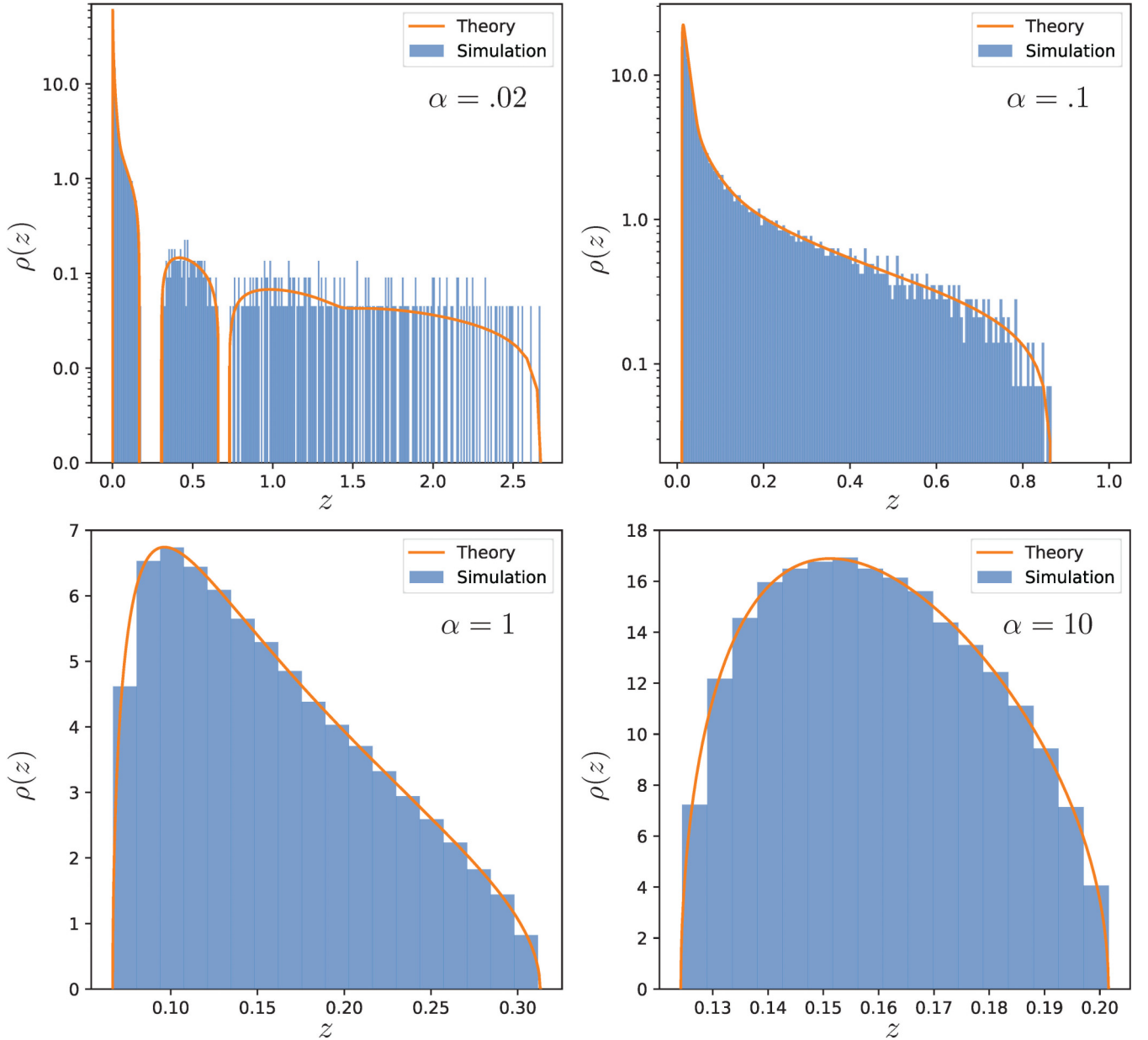
FIG. 3. Density of eigenvalues of **C**, without the extensive eigenvalue z_{ext}, for various values of α. Orange: Results from (38). Blue: Outputs of numerical diagonalization for $N = 2500$. Same model as in Fig. 2.

When α is sufficiently large, all connected components have merged into a single continuous, semicircle distribution, as could be expected from the vanishing correlation between the matrix elements of **C**, centered in $z_1 = \frac{1}{2}(z_- + z_+) = \hat{\Gamma}_1$ and of half-width $\frac{1}{2}(z_+ - z_-) = 2\sqrt{\hat{\Gamma}_2/\alpha}$, with $\hat{\Gamma}_1 = \sum_{\mathbf{k} \neq \mathbf{0}} \hat{\Gamma}(\mathbf{k})$ and $\hat{\Gamma}_2 = \sum_{\mathbf{k} \neq \mathbf{0}} \hat{\Gamma}(\mathbf{k})^2$.

C. Eigenvectors of MERM and Fourier modes associated to the ERMs

We briefly discuss here the properties of the eigenvectors of MERM. We consider a connected component of eigenvalues originated from the same ERM eigenvalue (labelled by $\mathbf{k}$), see previous section. To quantify how much the MERM eigenvectors **v** are related to the $2L$ eigenvectors (Fourier

modes) of the L ERMs, we write

$$v_i = \sum_{\ell=1}^{L} \left[\gamma_\ell \frac{1}{\sqrt{N}} \cos\left(2\pi \, \mathbf{k} \cdot \mathbf{r}_i^\ell\right) + \delta_\ell \frac{1}{\sqrt{N}} \sin\left(2\pi \, \mathbf{k} \cdot \mathbf{r}_i^\ell\right) \right]$$
$$+ R_i, \tag{46}$$

where γ_ℓ and δ_ℓ are the projection coefficients onto the $2L$ ERMs eigenvectors and **R** is the component of **v** orthogonal to this subspace.

The distributions of the coefficients γ_ℓ and δ_ℓ and of the norm of **R** are shown in Fig. 4 in the case $L = 5$ and for increasing values of N. We observe the following:

(i) The magnitude of γ_ℓ and δ_ℓ seems to be independent of N [Fig. 4(a)], which implies that these coefficients remain finite as $N \to \infty$. Conversely, the projections of **v** on Fourier

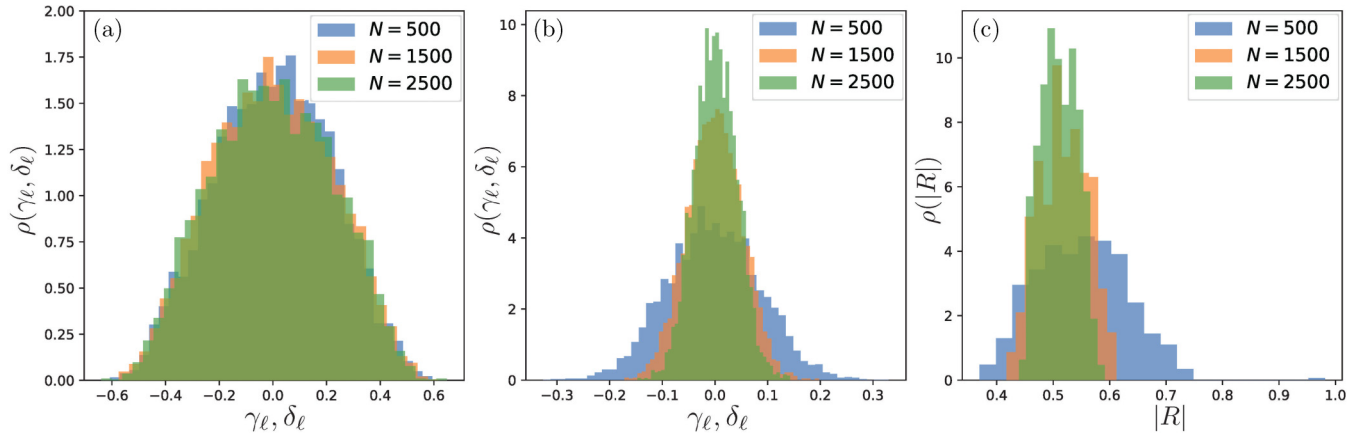FIG. 4. (a) Histogram of the coefficients γ_ℓ and δ_ℓ for different values of N. Results correspond to the $k = 1$ connected component of eigenvalues in dimension $D = 1$ and for $L = 5$ spaces, averaged over 50 samples. Same model as in Fig. 2. (b) Histograms of the projections of eigenvectors $\mathbf{v}$ to the $k = 2$ Fourier modes of the ERMs. (c) Histograms of the norm of the orthogonal component $\mathbf{R}$, see (46).

modes attached to a momentum $\mathbf{k}' \neq \mathbf{k}$ vanishes with increasing N, see Fig. 4(b). Hence, $\mathbf{v}$ retains some coherence with the $2L$ eigenvectors of the ERMs attached to the connected component even in the infinite size limit (provided L remains finite).

(ii) The norm of $\mathbf{R}$ seems to get peaked as N grows around a nonzero value. Therefore, $\mathbf{v}$ has a substantial component outside the $2L$-dimensional subspaces spanned by the ERM eigenmodes.

Notice that the magnitudes of the γ and δ coefficients and of the norm of $\mathbf{R}$ are related to each other through $\langle \gamma^2 \rangle = \langle \delta^2 \rangle = (1 - \langle \mathbf{R}^2 \rangle)/L$ to ensure the normalization of $\mathbf{v}$. The results above were derived for finite L and large N; in the double scaling limit where both L, N are large at fixed ratio α, we find that the coefficients γ, δ of the projections on the Fourier modes attached to the connected component also scale as $N^{-1/2}$, in accordance with the number of those modes.

V. VARIANTS OF MODEL

The function Γ we have considered so far corresponds to the simple model defined in Fig. 1. In a unit cube $\mathcal{H}_D$ in D dimensions, a set of N positions $\mathbf{r}_i^\ell$ (centers of D-dimensional spheres of volume $\phi_0 < 1$) are drawn uniformly and independently at random for each "map" ℓ.

The term $\Gamma(|\mathbf{r}_i^\ell - \mathbf{r}_j^\ell|)$ entering in the correlation matrix (2) is simply the overlap (common volume) between the two spheres in the same space, see Fig. 1. We consider below three variants of this model, of interest for computational neuroscience, see Sec. VI.

A. Dilution

Let us first consider single-space ERM in which a fraction ρ_0 of the N positions (chosen at random among $1, \ldots, N$) carry vanishingly small spheres, and the remaining points are centers of standard spheres of volume ϕ_0, see Fig. 5(a). All the entries of ERM $M_{ij}^{(1)} = \Gamma(|\mathbf{r}_i - \mathbf{r}_j|)/N$ such that i or j belongs to the first subset (with pointlike spheres) are equal to zero. We are left with a block matrix of dimension $(1 - \rho_0)N \times (1 - \rho_0)N$, equal to the ERMs considered so far

with the model of Fig. 1. As a consequence, in the large N limit, the eigenvalues of this block-ERM are equal to $\rho_0 \, \hat{\Gamma}(\mathbf{k})$, while the remaining eigenvalues are equal to zero.

The resolvent of this diluted version of ERM in the high-density regime has the same form as (7):

$$
s_1(z) = -\frac{1}{zN} \left[\rho_0 N + \sum_{\ell=1}^{\infty} \sum_{\substack{\mathbf{k} \neq \mathbf{0} \\ (|\mathbf{k}| \leqslant \rho_0 N)}} \hat{\Gamma}(\mathbf{k})^\ell \frac{1}{z^\ell} + (1 - \rho_0)N \right]
$$
$$
= -\frac{1}{z} - \frac{1}{Nz} \gamma\left(\frac{1}{z}\right), \tag{47}
$$

where

$$
\gamma(u) = \sum_{\mathbf{k} \neq \mathbf{0}} \frac{u \, \rho_0 \hat{\Gamma}(\mathbf{k})}{1 - u \, \rho_0 \hat{\Gamma}(\mathbf{k})} . \tag{48}
$$

The computation of the functional inverse of the resolvent of the dilute MERM can be done as in the standard case, and we get:

$$
z = \sum_{\mathbf{k} \neq \mathbf{0}} \frac{\alpha \, \rho_0 \hat{\Gamma}(\mathbf{k})}{\alpha + s \, \rho_0 \hat{\Gamma}(\mathbf{k})} - \frac{1}{s}. \tag{49}
$$

We can now solve equation (49) in order to get the density of eigenvalues. The agreement with the spectrum obtained from numerical simulations is excellent, see Fig. 5(d).

B. Spheres of different volumes

We now discuss the case of a multinomial distribution of sphere volumes. We consider first that, in each space, a fraction ρ_1 of the N spheres have volume ϕ_1, while the remaining fraction $\rho_2 = 1 - \rho_1$ have volume ϕ_2, see Fig. 5(b). For every space we build a matrix composed of four blocks:

$$
\mathbf{M}^{(1)} = \frac{1}{N} \left(\begin{array}{c|c} \mathbf{\Gamma}_{11} & \mathbf{\Gamma}_{12} \\ \hline \mathbf{\Gamma}_{21} & \mathbf{\Gamma}_{22} \end{array} \right), \tag{50}
$$

where the block $\mathbf{\Gamma}_{ab}$ is a $\rho_a N \times \rho_b N$ ERM depending on the overlaps between spheres of volumes ϕ_a and ϕ_b, and with a, b taking values 1 or 2. We look for eigenvectors of $\mathbf{M}^{(1)}$
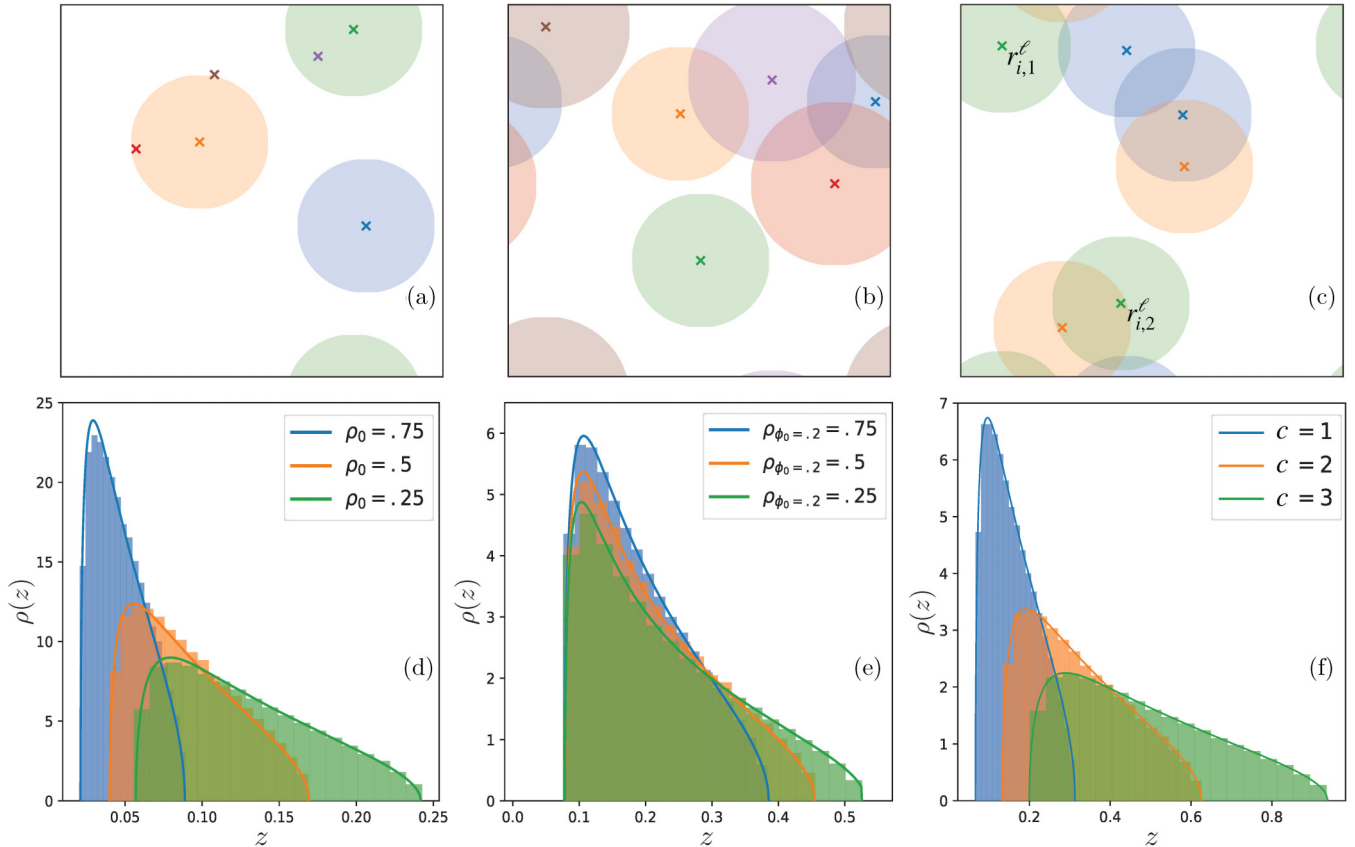
FIG. 5. Top panels: Sketches of the model variants, respectively (a) dilution, (b) spheres of different sizes and (c) multiple spheres. Bottom panels: (d) Density of eigenvalues for the MERM for $\phi_0 = 0.2$ with different dilution fractions ρ_0. (e) Density of eigenvalues of MERM with different fractions $\rho_{\phi_0=0.2}$ of spheres with volume $\phi_0 = 0.2$ and $\rho_{\phi_0=0.4}$ of spheres with volume $\phi_0 = 0.4$ in each space. (f) Density of eigenvalues of MERM for $\phi_0 = 0.2$ with $c = 2$ spheres for each index i in each map. Parameters: $N = 2500$, $D = 1$, $\alpha = 1$. In all cases we do not show the extensive eigenvalue.

of components $v_i(\mathbf{k}) \propto e^{i\,2\pi\,\mathbf{k}\cdot\mathbf{r}_i}$ multiplied by α_a for the sites i in the fraction ρ_a, with $a = 1, 2$. We obtain the following eigensystem :

$$\begin{cases} \rho_1\,\hat{\Gamma}_{11}(\mathbf{k})\,\alpha_1 + \rho_2\,\hat{\Gamma}_{12}(\mathbf{k})\,\alpha_2 = \lambda(\mathbf{k})\,\alpha_1 \\ \rho_1\,\hat{\Gamma}_{21}(\mathbf{k})\,\alpha_1 + \rho_2\,\hat{\Gamma}_{22}(\mathbf{k})\,\alpha_2 = \lambda(\mathbf{k})\,\alpha_2 \end{cases}. \quad (51)$$

In the system above $\hat{\Gamma}_{ab}(\mathbf{k}) = \hat{\gamma}_a(\mathbf{k})\hat{\gamma}_b(\mathbf{k})$ with a, b taking value 1 or 2 and

$$\hat{\gamma}_a(\mathbf{k}) = \int_{\mathcal{H}_D} d\mathbf{r}\, \gamma_a(\mathbf{r})\, e^{-i2\pi\mathbf{k}\cdot\mathbf{r}} \quad (52)$$

with $\gamma_a(\mathbf{r})$ being the indicator function of the place field of volume ϕ_a. We find $\alpha_a \propto \hat{\gamma}_a(\mathbf{k})$ and $\lambda(\mathbf{k}) = \rho_1[\hat{\gamma}_1(\mathbf{k})]^2 + \rho_2[\hat{\gamma}_2(\mathbf{k})]^2$.

This result immediately extends to more than two sphere types. If we have K finite (as $N \to \infty$) types of spheres, with associated volumes ϕ_a and fractions ρ_a, with $a = 1, \ldots, K$, then the eigenvalue of ERM attached to the momemtum $\mathbf{k}$ is given by

$$\lambda(\mathbf{k}) = \sum_{a=1}^{K} \rho_a\, [\hat{\gamma}(\mathbf{k})]^2. \quad (53)$$

It is straightforward to write the resulting self-consistent equation for the MERM resolvent by simply changing $\hat{\Gamma}(\mathbf{k}) \to$

$\sum_{a=1}^{K} \rho_a\, [\hat{\gamma}_{aa}(\mathbf{k})]^2$ in (19). In Fig. 5(e) we show the perfect agreement of this theoretical result with numerical simulations.

C. Multiple spheres per site in each space

We extend the above setting to the case of multiple spheres per site in each space. More precisely, we assume that for each site $i = 1, \ldots, N$, there are c centers $\mathbf{r}_{i,m}^{\ell}$ of spheres, with $m = 1, \ldots, c$ in each space ℓ, see Fig. 5(c); we assume that c remains finite as N, L are sent to infinity. The MERM is defined as follows

$$C_{ij} = \frac{1}{L} \sum_{\ell=1}^{L} \sum_{m,m'=1}^{c} \Gamma\big(|\mathbf{r}_{i,m}^{\ell} - \mathbf{r}_{j,m'}^{\ell}|\big). \quad (54)$$

To better understand what happens in this case we consider the limit case of a single map:

$$M_{ij}^{(1)} = \frac{1}{N} \sum_{m,m'=1}^{c} \Gamma(|\mathbf{r}_{i,m} - \mathbf{r}_{j,m'}|). \quad (55)$$

In the high-density regime the eigenvectors of this ERM have components $v_i(\mathbf{k}) \propto \sum_m e^{i\,2\pi\,\mathbf{k}\cdot\mathbf{r}_{i,m}}$ with eigenvalues equal to $c\,\hat{\Gamma}(\mathbf{k})$ (for $\mathbf{k} \neq \mathbf{0}$). The only change to the functional inverse

of the MERM resolvent is $\hat{\Gamma}(\mathbf{k}) \rightarrow c\,\hat{\Gamma}(\mathbf{k})$, so that we obtain:

$$z = \sum_{\mathbf{k} \neq \mathbf{0}} \frac{\alpha\, c\, \hat{\Gamma}(\mathbf{k})}{\alpha + s\, c\, \hat{\Gamma}(\mathbf{k})} - \frac{1}{s} . \tag{56}$$

We have solved Eq. (56) in order to get the density of eigenvalues; results are in excellent agreement with numerics, see Fig. 5(f).

VI. CONCLUSION

In this work we have introduced a novel statistical ensemble for ERM, where the element i, j of the matrix depend on the distances between representative points of i and j in more than one space. Using a combination of heuristic assumptions and analytical and numerical calculation, we have shown that the high-density limit is nontrivial when the number L of spaces and the size N of the matrix are sent to infinity, with a fixed ratio $\alpha = L/N$. We have analytically studied the density of eigenvalues of this MERM ensemble, based on free-probability identities and on the replica method. Our results are in very good agreement with numerical simulations for all the cases we have considered. We stress that our results are, at this stage, not rigorous, and we hope that mathematical studies will focus on MERM properties in future.

Our motivation to introduce and study MERM came from computational neuroscience [14], in particular the modeling of spatial representations in the mammalian hippocampus. The activity of place cells strongly depends on the position of the animal in the environment, defining spatial place fields in which they are active. Experiments on rodents and bats show that place fields are approximately disks in two-dimensional environments and spheres in three dimensions. Our basic model, shown in Fig. 1, assumes that all place fields cover the same area or volume. However, in the CA3 region of the hippocampus in particular, neurons may have place fields in some environment and none in other environments, which

corresponds to the dilute model introduced in Sec. V. In addition, we have introduced other variants, in which the radius of place fields varies or a place field is made of more than one connected spatial component, as seen in large environments [21]. While the variants of the model considered here lead to different densities of eigenvalues z, the behaviours of these densities for $z \rightarrow 0$ and $\alpha \rightarrow 0$ seem qualitatively robust, which suggests that the storage capacity of recurrent neural networks is a robust property of the space-to-neural activity encoding [14].

In addition to the neuroscience motivation reported above, we hope that MERM will find applications and be of interest in other fields, i.e., in applied mathematics or in information theory. In particular, our results could be used for functions Γ with a dependence on the pairwise distances different from the ones considered in this article. From a random matrix point of view, it would also be natural to consider models for MERM, where the statistical features of the L ERM's are non-independent from space to space. In the context of place cells and fields, it is known that neurons have some individuality, that is, retain some properties in the different environments. In particular it was reported experimentally [21,22] that each place cell has its own propensity to have one place field per square meter: many neurons have very low propensity values, i.e., have no place field at all in many maps as in Fig. 5(a), and few neurons that have very high propensity and therefore tend to code almost all maps even with more than one place field connected component per map [Fig. 5(c)]. It would be very interesting to study the consequences of nonindependence between the elementary ERMs composing the MERM on the density of eigenvalues and the structure of the eigenvectors.

ACKNOWLEDGMENTS

[1] M. Mézard, G. Parisi, and A. Zee, Spectra of Euclidean random matrices, Nucl. Phys. B **559**, 689 (1999).

[2] S. E. Skipetrov and A. Goetschy, Eigenvalue distributions of large Euclidean random matrices for waves in random media, J. Phys. A: Math. Theor. **44**, 065102 (2011).

[3] C. Bordenave, Eigenvalues of Euclidean random matrices, Rand. Struct. Algor. **33**, 515 (2008).

[4] N. El Karoui, The spectrum of kernel random matrices, Ann. Stat. **38**, 1 (2010).

[5] R. Couillet and F. Benaych-Georges, Kernel spectral clustering of large dimensional data, Electr. J. Stat. **10**, 1393 (2016).

[6] G. Parisi, Euclidean random matrices, the glass transition and the boson peak, Eur. Phys. J. E **9**, 213 (2002).

[7] T. S. Grigera, V. Martin-Mayor, G. Parisi, and P. Verrocchio, Vibrations in glasses and Euclidean random matrix theory, J. Phys.: Condens. Matter **14**, 2167 (2002).

[8] T. S. Grigera, V. Martin-Mayor, G. Parisi, P. Urbani, and P. Verrocchio, On the high-density expansion for Euclidean random matrices, J. Stat. Mech. (2011) P02015.

[9] A. Goetschy and S. E. Skipetrov, Non-Hermitian Euclidean random matrix theory, Phys. Rev. E **84**, 011150 (2011).

[10] S. Ciliberti, T. S. Grigera, V. Martn-Mayor, G. Parisi, and P. Verrocchio, Anderson localization in Euclidean random matrices, Phys. Rev. B **71**, 153104 (2005).

[11] A. Amir, Y. Oreg, and Y. Imry, Localization, Anomalous Diffusion, and Slow Relaxations: A Random Distance Matrix Approach, Phys. Rev. Lett. **105**, 070601 (2010).

[12] A. Goetschy and S. E. Skipetrov, Euclidean random matrices and their applications in physics, arXiv:1303.2880 (2013).

[13] E. I. Moser, E. Kropff, and M. B. Moser, Place cells, grid cells, and the brain's spatial representation system, Annu. Rev. Neurosci. **31**, 69 (2008).

[14] A. Battista and R. Monasson, Capacity-Resolution Trade-Off in the Optimal Learning of Multiple Low-Dimensional Manifolds by Attractor Neural Networks, Phys. Rev. Lett. **124**, 048302 (2020).

[15] C. B. Alme *et al.*, Place cells in the hippocampus: eleven maps for eleven rooms, Proc. Natl. Acad. Sci. USA **111**, 18428 (2014).

[16] K. Jezek *et al.*, Theta-paced flickering between place-cell maps in the hippocampus, Nature **478**, 246 (2011).

[17] N. Brunel, Is cortical connectivity optimized for storing information?, Nat. Neurosci. **19**, 749 (2016).

[18] G. Livan, M. Novaes, and P. Vivo, *Introduction to Random Matrices: Theory and Practice* (Springer International, Cham, 2018).

[19] J. A. Mingo and R. Speicher, *Free Probability and Random Matrices*, Vol. 35 (Springer, New York, 2017).

[20] M. Mézard, G. Parisi, and M. Virasoro, *Spin Glass Theory and Beyond: An Introduction to the Replica Method and Its Applications*, Vol. 9 (World Scientific, Singapore, 1987).

[21] P. D. Rich, H. P. Liaw, and A. K. Lee, Large environments reveal the statistical structure governing hippocampal representations, Science **345**, 814 (2014).

[22] J. S. Lee, J. Briguglio, S. Romani, and A. K. Lee, The statistical structure of the hippocampal code for space as a function of time, context, and value, bioRxiv 615203 (2019).